Self-imaging generation of plasmonic void arrays

Wang, Rong (EEE); Wei, Shibiao; Lin, Jiao; Wang, Qian; Yuan, Guanghui; Du, Luping; Wang, Yanqin; Luo, Xiangang; Hong, Minghui; Min, Changjun; Yuan, Xiaocong

2013

Wei, S., Lin, J., Wang, R., Wang, Q., Yuan, G., Du, L., Wang, Y., Luo, X., Hong, M., Min, C.,& Yuan, X. (2013). Self-imaging generation of plasmonic void arrays. Optics Letters, 38(15), 2783-2785.

https://hdl.handle.net/10356/98145

https://doi.org/10.1364/OL.38.002783

Self-imaging generation of plasmonic void arrays

Shibiao Wei,[1] Jiao Lin,[2,7] Rong Wang,[1] Qian Wang,[3] Guanghui Yuan,[3] Luping Du,[3] Yanqin Wang,[4] Xiangang Luo,[4] Minghui Hong,[5] Changjun Min,[1] and Xiaocong Yuan[6,8]

[1]*Institute of Modern Optics, Key Laboratory of Optical Information Science & Technology, Ministry of Education of China, Nankai University, Tianjin 300071, China*

[2]*School of Physics, University of Melbourne, VIC 3010, Australia*

[3]*School of Electrical & Electronic Engineering, Nanyang Technological University, Nanyang Avenue, Singapore 639798*

[4]*Institute of Optics and Electronics, Chinese Academy of Sciences, State Key Laboratory for Optical Technologies of Microfabrication, Chengdu 610209, China*

[5]*Department of Electrical and Computer Engineering, National University of Singapore, 4 Engineering Drive 3, Singapore 117576*

[6]*Institute of Micro & Nano Optics, Shenzhen University, Shenzhen 518060, China*

[7]*e-mail: jiao.lin@unimelb.edu.au*

[8]*e-mail: xcyuan@szu.edu.cn*

Received April 2, 2013; revised June 24, 2013; accepted June 24, 2013; posted June 27, 2013 (Doc. ID 188171); published July 29, 2013

A plasmonic device is proposed to produce a self-imaging surface plasmon void array (2D surface bottle beam array) by the interference of two nondiffracting surface beams, namely, cosine-Gauss beams. The self-imaging surface voids are shown by full-wave calculations and then verified experimentally with an aperture-type near-field scanning optical microscope. We also demonstrate that the void array can be adjusted with flexibility in terms of the pattern and the number of voids. © 2013 Optical Society of America

OCIS codes: (070.6760) Talbot and self-imaging effects; (240.6680) Surface plasmons; (250.5403) Plasmonics.
http://dx.doi.org/10.1364/OL.38.002783

Optical voids, that is, low or null intensity regions in an optical field enclosed by higher intensity, have found numerous applications in recent years; for example intensity minima in a focused optical field were used to trap microparticles with low refractive indices in optical tweezers [1,2]. In a trap of atoms (laser cooling), if the trapping beam is blue-detuned from the resonant transition of the atoms, they will be confined by repulsive forces in the dark region [3,4]. A popular choice for the generation of optical voids is to use vortex beams that have a two-dimensional (2D) on-axis intensity minimum in the transverse plane throughout propagation [5]. Bottle beams, on the other hand, offer three-dimensional (3D) voids with additional intensity variation in the propagation axis. Arlt and Padgett first constructed a bottle beam with a 3D intensity void from the interference of two phased Laguerre–Gaussian modes, LG_{00} and LG_{20}, by using a computer-generated hologram [6]. Recently, various other types of bottle beams have been explored, for instance, a 3D dark focus [7], bottle beams with long nondiffracting distance [8], holographic optical bottle beams [9], and vortex bottle beams carrying orbital angular momentum [10]. It is noted, however, that all these bottle beams were generated for free-space applications. In this Letter, we extend the concept of bottle beams to surface waves by introducing a plasmonic device that generates an array of surface plasmon (SP) voids (2D bottle beams) tightly bound to an air–metal interface by the use of the self-imaging effect. In addition, we show that both the patterns and the number of SP voids are adjustable by varying the design of this plasmonic device.

The Talbot effect, that is, the self-imaging effect, was first observed in the study of transmission gratings and arrays of holes perforated in metal films [11]. With the self-imaging effect, an optical field repeats at a regular interval known as the Talbot length. However, it has been shown that the self-imaging effect can be created by the superposition of a proper set of nondiffracting beams in free-space without periodic structures like gratings [12]. A nondiffracting beam maintains its transverse profile as it propagates in free space. In this case, the self-imaging effect occurs when the propagation constants of the constituent nondiffracting beams are different. So the beating among different propagation constants results in periodically constructive interference and destructive interference forming the repeated optical field along the propagating direction [13]. In our study, this phenomenon is used to ensure that all the constituent SP voids in the near-field array have comparable sizes. In particular, the superposition of two nondiffracting surface waves, namely cosine-Gauss beams (CGB) [14], is employed to produce the self-imaging void arrays. A nondiffracting CGB can be generated by interfering two SP plane waves at half-intersecting angle θ, shown in Fig. 1(a). The resultant 2D nondiffracting surface wave is characterized by

$$E_z(x,y) = E_0 \cos(k_y y) \exp(-y^2/w_0^2) \exp(ik_x x), \quad (1)$$

where E_0 is a complex constant, and w_0 denotes the beam waist in the y direction. k_x and k_y are the x and y components of the SP plane wave propagation constant k_{sp}, respectively.

Two collinear CGBs with different half-intersecting angles θ_1 and θ_2 are generated simultaneously to create the self-imaging SP void array at the region where the two beams overlap with each other. The design scheme is shown in Fig. 1(b). Two SP line sources (solid red) with

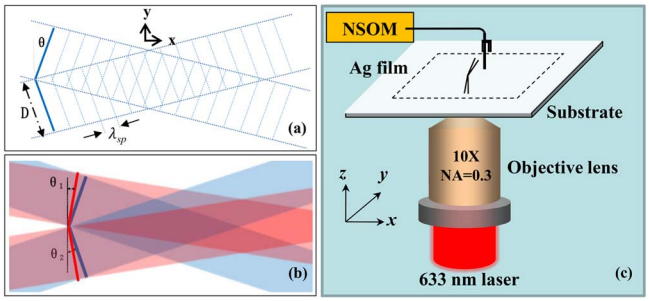

Fig. 1. Schematic of the designed structure. (a) A nondiffracting CGB is generated by interfering two SP plane waves at half-intersecting angle θ; blue solid lines represent SP line sources. (b) Arrays of plasmon bottle beams constructed by interfering two nondiffracting CGBs. The red and blue solid lines represent SP line sources with a length of D with varying half-intersecting angles θ_1 and θ_2. Two CGBs with varying propagating constants in the propagating direction are generated, which then interfere with each other within the overlap area, forming an array of voids. (c) Experimental setup. A Gaussian beam from a linearly polarized 633 nm laser source (x polarized), focused by an objective lens (10×, NA = 0.3), normally incident on the metal surface to excite SP waves. The aperture-type near-field scanning optical microscope (NSOM) with an aluminum-coated fiber tip (tip aperture about 100 nm in diameter) is used to measure the 2D SP field distribution.

intersecting angle θ_1 on the left-hand side generates a CGB with the propagation constant labeled k_{x1}, while the other two SP line sources (solid blue) on the right-hand side generated another CGB with a different propagation constant k_{x2}. It is noted that, ideally, $k_{x1} = k_{\mathrm{sp}} \cos(\theta_1)$ and $k_{x2} = k_{\mathrm{sp}} \cos(\theta_2)$. The resultant 2D amplitude distribution of the superposition can thus be expressed as

$$\begin{aligned} E'_z(x,y) &= E_{z1}(x,y) + E_{z2}(x,y) \\ &= E_1 \cos(k_{y1}y)\exp(-y^2/w_0^2)\exp(ik_{x1}x) \\ &\quad + E_2 \cos(k_{y2}y)\exp(-y^2/w_0^2)\exp(ik_{x2}x). \end{aligned} \quad (2)$$

We show the self-imaging property (periodicity in the propagation direction) of the field by considering the variation of the on-axis ($y = 0$) intensity. Also, the propagation constant of SP waves can be expressed in terms of its real and imaginary components as $k_{\mathrm{sp}} = k'_{\mathrm{sp}} + ik''_{\mathrm{sp}}$. The approximation $E_1 \cong E_2 = E_0$ is used in Eq. (2), while the half-intersecting angles θ_1 and θ_2 are small. Therefore we have the on-axis intensity component distribution of SP waves expressed as

$$\begin{aligned} I(x,0) &= E'_z(x,0)E'^{*}_z(x,0) \\ &= |E_0|^2\{\exp(-2k''_{x1}x) + \exp(-2k''_{x2}x) \\ &\quad + 2\cos[(k'_{x1} - k'_{x2})x]\exp[-(k''_{x1} + k''_{x2})x]\}. \end{aligned} \quad (3)$$

The three exponents in Eq. (3) indicate the inherent Ohmic propagation loss of SP waves. The sinusoidal intensity variation represented by the third term of Eq. (3) is the result of the beating of two different propagation constants of CGBs in the x axis. Therefore, the period of the SP bottle array, depending on the cosine function in Eq. (3), is given by $T = \lambda_{\mathrm{sp}}/(\cos\theta_1 - \cos\theta_2)$ within the overlapped region along the x axis, where

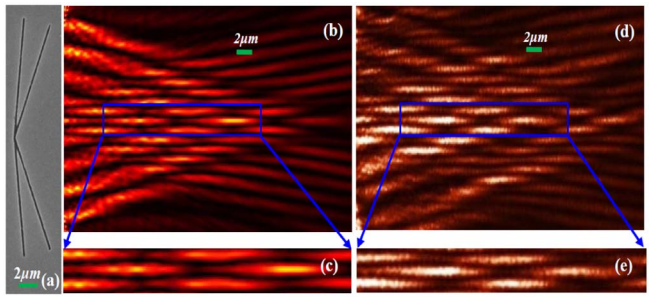

Fig. 2. Arrays of voids generated by interference of two CGBs. (a) Scanning electron micrograph of the sample. (b) Finite-difference time-domain (FDTD) numerical calculation and (d) the near-field SP intensity distributions obtained from experimental measurement by NSOM. Two typical voids surrounded by high intensities are shown in (c) and (e), corresponding to areas outlined by blue frames in (b) and (d), respectively.

$$\lambda_{\mathrm{sp}} = \lambda_0\sqrt{\frac{\varepsilon_d + \varepsilon_m}{\varepsilon_d\varepsilon_m}} \quad (4)$$

is the wavelength of SP waves. λ_0 is the wavelength (633 nm) of the incident light. ε_d and ε_m are dielectric constants of the metal (Ag) and the medium (air), respectively.

Two pairs of grooves [Fig. 2(a)] with different half-intersecting angles were fabricated in a silver film on a glass substrate by focused ion beam milling to generate two CGBs with different propagating constants. The optically opaque silver film is 300 nm thick to avoid the interference caused by the directly transmitted incident light and the SP waves. In the example illustrated in Fig. 2, the half-angles θ were chosen to be 5° and 20°, respectively, and the length of grooves D was set to be 10 μm for both constituent CGBs.

One can see that an array of self-imaging voids [two of them are isolated by the blue boxes and are shown in Figs. 2(c) and 2(e)] is obtained because of the self-imaging effect as a result of the interference of two nondiffracting CGBs. As a π phase jump exists between adjacent transverse intensity maxima of a CGB, there is half-period shift in the propagation direction for the intensity pattern across the y axis, which results in an intensity variation in the transverse direction. Numerical modeling of the near-field intensity distribution of the SP void array was performed with full-wave calculations based on the finite-difference time-domain (FDTD) method. The experimentally observed near-field intensity distribution [Figs. 2(d) and 2(e)] are in good agreement with the numerical calculations [Figs. 2(b) and 2(c)].

We further demonstrate that both the patterns and the number of voids can be controlled by varying the design of the plasmonic device. In Fig. 3, we give two designs [$D = 15$ μm, $\theta_1 = 10°$, and $\theta_2 = 20°$, shown in Figs. 3(b) and 3(c), $\theta_1 = 5°$ and $\theta_2 = 30°$ shown in Figs. 3(d) and 3(e)], in which the length of grooves and the half-intersecting angles are different from those in the previous example (Fig. 2) while the rest of the parameters remain the same. The distance of the self-imaging area (area of array voids) depends on the minimum nondiffracting distance of the two CGBs. In our case, the distance of the

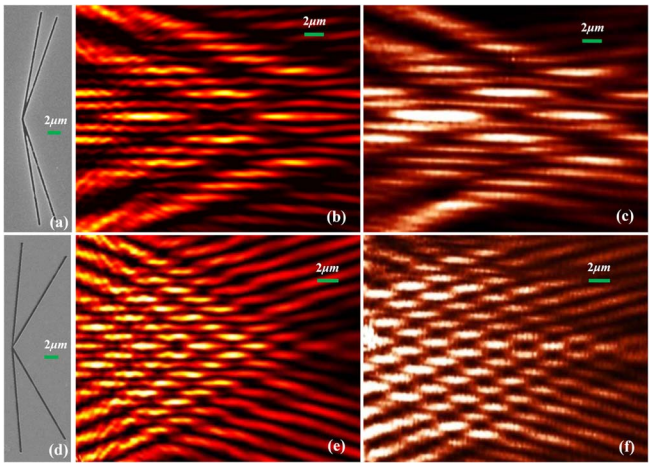

Fig. 3. Scanning electron micrograph of device with (a) $D = 15$ μm, $\theta_1 = 10°$, $\theta_2 = 20°$; (d) $D = 15$ μm, $\theta_1 = 5°$, $\theta_2 = 30°$. (b) and (e) FDTD simulation; (c) and (f) NSOM measurement. Intensity distributions of void arrays with different parameters: (b) and (c) with $\theta_1 = 10°$, $\theta_2 = 20°$, $D = 15$ μm; (e) and (f) with $\theta_1 = 5°$, $\theta_2 = 30°$, $D = 15$ μm.

self-imaging area is $x = D/\sin(\theta_2)$. Taking the periodicity of the plasmonic voids propagating in the x direction, $\lambda_{SP}/(\cos\theta_1 - \cos\theta_2)$, into consideration, the number of on-axis plasmonic voids is $N = D(\cos\theta_1 - \cos\theta_2)/(\lambda_{SP}\sin\theta_2)$. In the simulations and the experiments, shown in Figs. 3(b), 3(e) and 3(c), 3(f), both the periodicity and the number of voids are determined by the half-intersecting angles θ_1 and θ_2. The theoretical periodicities of the plasmonic voids shown in Figs. 3(a) and 3(b) are 13.6 and 4.7 μm, which are close to the experimentally measured 13.9 and 4.9 μm.

In conclusion, we have shown that plasmonic voids can be generated by the self-imaging effect with a plasmonic device consisting of two pairs of intersecting grooves fabricated by focused ion beam milling on the surface of silver film. This phenomenon is based on the superposition of two nondiffraction CGBs generated by two pairs of grooves. The full-wave simulation and experimental results obtained by NSOM are in good agreement, and the results indicated that all the constituent SP voids in the near-field array had comparable sizes. Furthermore, we verified that both the pattern and the number of voids could be adjusted by simply varying the intersecting angles and the length of SP sources. This controllable property of SP void patterns could be useful toward developing plasmonic-based nanophotonics devices and planar plasmonic circuits. The 2D arrays of SP voids have great potential in the applications of near field optical trapping in terms of noninvasive manipulation [15,16], sorting 2D near-field particles [17,18], and laser cooling techniques [19,20].

This work was partially supported by the National Natural Science Foundation of China under grants 61036013, 61138003, and 11204141. X. C. Yuan acknowledges the support given by the Ministry of Science and Technology of China under grant 2009DFA52300 for China–Singapore collaborations, the National Research Foundation of Singapore under grant NRF-G-CRP2007-01, and Tianjin Municipal Science and Technology Commission under grant 11JCZDJC15200. J. Lin is the recipient of the Discovery Early Career Researcher Award funded by the Australian Research Council under project DE130100954. J. Lin acknowledges the financial support from the Defence Science Institute, Australia.

References

1. K. T. Gahagan and G. A. Swartzlander, Opt. Lett. **21**, 827 (1996).
2. K. T. Gahagan and G. A. Swartzlander, J. Opt. Soc. Am. B **16**, 533 (1999).
3. T. Puppe, I. Schuster, A. Grothe, A. Kubanek, K. Murr, P. W. H. Pinkse, and G. Rempe, Phys. Rev. Lett. **99**, 013002 (2007).
4. G. Li, S. Zhang, L. Isenhower, K. Maller, and M. Saffman, Opt. Lett. **37**, 851 (2012).
5. L. Allen, M. W. Beijersbergen, R. J. C. Spreeuw, and J. P. Woerdman, Phys. Rev. A **45**, 8185 (1992).
6. J. Arlt and M. J. Padgett, Opt. Lett. **25**, 191 (2000).
7. D. Yelin, B. E. Bouma, and G. J. Tearney, Opt. Lett. **29**, 661 (2004).
8. B. P. S. Ahluwalia, X.-C. Yuan, and S. H. Tao, Opt. Commun. **238**, 177 (2004).
9. C. Alpmann, M. Esseling, P. Rose, and C. Denz, Appl. Phys. Lett. **100**, 111101 (2012).
10. J. Arlt and M. J. Padgett, Opt. Commun. **281**, 1358 (2008).
11. H. F. Talbot, Philos. Mag. **9**(56), 401 (1836).
12. P. Szwaykowski and J. Ojeda-Castaneda, Opt. Commun. **83**, 1 (1991).
13. Z. Bouchal, Czech. J. Phys. **53**, 537 (2003).
14. J. Lin, J. Dellinger, P. Genevet, B. Cluzel, F. de Founel, and F. Capasso, Phys. Rev. Lett. **109**, 093904 (2012).
15. M. Righini, G. Volpe, C. Girard, D. Petrov, and R. Quidant, Phys. Rev. Lett. **100**, 186804 (2008).
16. K. Wang, E. Schonbrun, P. Steinvurzel, and K. B. Crozier, Nano Lett. **10**, 3506 (2010).
17. T. Cizmar, M. Siler, M. Sery, and P. Zemanek, Phys. Rev. B **74**, 035105 (2006).
18. M. Righini, A. S. Zelenina, C. Girard, and R. Quidant, Nat. Phys. **3**, 477 (2007).
19. E. S. Shuman, J. F. Barry, and D. DeMille, Nature **467**, 820 (2010).
20. V. Vuletic and S. Chu, Phys. Rev. Lett. **84**, 3787 (2000).